

THE COLOR-ABSOLUTE MAGNITUDE RELATION FOR E AND S0 GALAXIES.  
 I. CALIBRATION AND TESTS FOR UNIVERSALITY USING VIRGO AND  
 EIGHT OTHER NEARBY CLUSTERS

NATARAJAN VISVANATHAN

Hale Observatories, Carnegie Institution of Washington, California Institute of Technology, and Mount Stromlo  
 and Siding Spring Observatories, Research School of Physical Sciences, Australian National University

AND

ALLAN SANDAGE

Hale Observatories, Carnegie Institution of Washington, California Institute of Technology

Received 1977 January 14

ABSTRACT

Spectrum scanner observations of E and S0 galaxies in the Virgo cluster confirm the previously known correlation between color and absolute magnitude, and show it to be strongly wavelength-dependent, with a maximum near  $\lambda 3500$ . Observations with discrete filter bands show a tight relation between  $u - V$  color ( $\langle \lambda \rangle 3500 \text{ \AA}$  and  $5500 \text{ \AA}$ ) and absolute visual magnitude, in the sense of bluer colors for fainter galaxies. The color-magnitude (C-M) gradient is 0.1 mag color change in  $u - V$  per unit absolute magnitude change, and is the same for E and S0 galaxies.

Galaxies in eight other groups and clusters show a color-magnitude effect that has the same wavelength dependence, slope, absolute magnitude calibration, and cosmic scatter as the Virgo cluster.

The C-M effect in all groups and clusters studied here can be made to coincide to form a common composite C-M correlation by shifts in magnitudes that are in the ratio of the redshifts ( $5 \log v/v_{\text{VIRGO}}$ ), which demonstrates the universality of the C-M effect, assuming that the local velocity-distance relation is linear.

On the other hand, if the magnitude shifts are determined independently by forcing the individual C-M relations to coincide with that for the Virgo cluster, photometric distances relative to Virgo can be determined that are redshift-independent. Such distances to nine groups and clusters correlate well with the redshifts, showing that the velocity-distance relation is linear, on the assumption now that the absolute magnitude calibration of the C-M effect is universal.

The Virgo cluster falls within  $25 \text{ km s}^{-1}$  of the ridge-line solution of the velocity-distance relation. This is within a velocity residual of  $0.3 \sigma$  of the variance of the mean velocity of the cluster itself ( $\sigma = 68 \text{ km s}^{-1}$ ). From these data, the Virgo cluster appears to have no measurable peculiar motion at a level of  $\sim 25 \text{ km s}^{-1}$  relative to the underlying uniform Hubble flow.

If we adopt the Virgo cluster modulus to be  $m - M = 31.70$ , the absolute calibration of the C-M effect for E and S0 galaxies becomes

$$M_{V_{26}^c} = -10.327(u - V)_c + 2.19,$$

with an intrinsic dispersion of  $\sigma(M) = \pm 0.5 \text{ mag}$  for a single galaxy. Hence photometric distances can be determined for single E and S0 galaxies by the color-magnitude method within errors that are distributed as  $\sigma(\delta r/r) = \pm 0.22$ .

*Subject headings:* galaxies: clusters of — galaxies: photometry

I. INTRODUCTION

A convincing measurement of departures of the velocity field from an ideal Hubble flow for very local galaxies (i.e., with  $v \lesssim 2000 \text{ km s}^{-1}$ ) would be of first importance in understanding the gravitational effects of density contrasts (clustering) on the local expansion rate, and hence of the role of gravity in specifying the global world model (Sandage, Tammann, and Hardy 1972; Silk 1974). However, existing claims for local velocity perturbations are controversial (de Vaucouleurs 1958, 1976; Sandage and Tammann 1975;

Sandage 1975; Peebles 1976; Rubin *et al.* 1976), and the question is evidently yet to be answered.

The observational problem consists of determining distances by methods that are independent of the redshift for a large sample of local galaxies, chosen in a specified manner so that selection effects can be accounted for.

Most of the recent discussions have been concerned with spiral galaxies whose statistical distances can be obtained with van den Bergh's method of luminosity classes (1960), suitably calibrated.

In the present series of papers, of which this is the

first, we begin to explore the possibility of using nearby E and S0 galaxies to map the velocity field by using the correlation between absolute magnitude and ultraviolet colors that was established earlier for particular samples of these types of systems (Baum 1959; Code 1959; de Vaucouleurs 1961; McClure and van den Bergh 1968; Lasker 1970; Sandage 1972*a*; de Vaucouleurs and de Vaucouleurs 1972; Faber 1973). Because there are sufficient numbers of bright E and S0 galaxies to the magnitude limit of the Shapley-Ames (1932) catalog, this independent mapping of the local velocity field seems feasible, provided that (1) the color-absolute magnitude effect can be shown to apply to all E and S0 galaxies in clusters, groups, and the general field (i.e., to be universal), and (2) the relation can be adequately calibrated.

As a first step toward answering these questions, we have undertaken an observational program to acquire low-resolution spectral scanner observations in the wavelength range from  $\lambda\lambda 3466$  to  $6730$  for many E and S0 galaxies in the Virgo cluster so as to study the wavelength dependence of the color-magnitude (C-M) effect itself. This enabled us to identify the wavelengths at which the C-M effect reaches a maximum, and hence to form a new and more efficient intermediate-band filter system incorporating these wavelengths.

Tests for universality of the C-M effect were then made by comparing the intermediate-band results for the Virgo cluster with those for other groups and clusters. These data and discussions are set out in the present paper.

The intermediate-band photometry has been obtained for most of the Shapley-Ames E and S0 galaxies in clusters, in groups, and in the field, and will be given in the forthcoming Paper II of the series, with a discussion of color-aperture effects and the dependence of reddening on galactic latitude.

The final two papers will deal with the Hubble diagram for the nearly complete sample of Shapley-Ames E and S0 galaxies (Paper III) and with the local velocity field itself (Paper IV).

## II. WAVELENGTH DEPENDENCE OF THE COLOR-ABSOLUTE MAGNITUDE EFFECT IN THE VIRGO CLUSTER

### *a) Instrument and Observational Procedure*

Previous work by Baum (1959), de Vaucouleurs (1961), Lasker (1970), and others listed in § I had shown that the change of color with absolute magnitude for E and S0 galaxies is greatest in the ultraviolet, and decreases markedly in the blue and visual regions. As just mentioned, we wished at the outset to determine more precisely this wavelength dependence so as to optimize the new intermediate-band color system we later used. To this end, energy distributions from  $\lambda\lambda 3466$  to  $7000$  were obtained during the spring of 1973 for Virgo cluster galaxies in the magnitude range  $8.7 < V < 14.0$ , using an automatic scanner (Visvanathan 1972; Visvanathan and Griensmith 1977).

The analyzing element of the scanner was a 4 inch (10.2 cm) semicircular continuous interference filter

that was mounted in the first half of a filter wheel and rotated by a stepping motor. The wavelength range of the filter was from  $\lambda\lambda 3600$  to  $7200$ , and the bandwidth at any given discrete position was  $\Delta\lambda/\lambda \approx 0.03$ . The relation between the observed wavelength and the angle through which the filter was rotated is linear, and the calibration of the wavelength points was obtained by known spectral lines. The observations were made from  $\lambda\lambda 3686$  to  $7045$  in steps of  $73 \text{ \AA}$ , and were extended to shorter wavelengths with two discrete narrow-band filters centered at  $\lambda\lambda 3466$  and  $3625$  that were mounted in the second half of the filter wheel. The bandwidths of these latter two separate filters are  $200$  and  $100 \text{ \AA}$ , respectively.

A preprogrammed electronic control unit was used to rotate the filter wheel to the desired wavelength, and also to select the exposure time at any part of the filter to a particular desired value. One unit of exposure time was  $15.5 \text{ ms}$ , which was controlled by the crystal clock in the Fabritek 1050 series computer. A provision to vary the exposure time from 4 to 256 units, in steps of two, was built in.

The stepping motor was programmed to dwell at each wavelength of the continuous filter and the two discrete filters for predetermined times (which varied from 128 units in the ultraviolet region to 8 units in the red region) so as to make the photon counts (galaxy + scanner + photomultiplier) nearly independent of wavelength. The total time for one scan was kept at 16 s, which tended to minimize the effect of transparency changes on the color measurements. To keep control on the variation of the sky, the number of scans for any one observation was kept small (usually 16 or 32), and also the galaxy observation was always preceded and succeeded by the sky observations.

The scanner was used in single-aperture mode through a focal-plane aperture of diameter  $30''$  at the Cassegrain focus of the Palomar 1.5 m telescope. The detector was an ITT FW S-20 photomultiplier, and pulse counting was used for all the observations.

The net galaxy counts in each wavelength were obtained, converted into magnitude, and reduced to outside the Earth's atmosphere in the conventional way. The sky was calculated from the two sky observations which bracket the galaxy observation. The absolute flux in  $\text{ergs s}^{-1} \text{ cm}^{-2} \text{ Hz}^{-1}$  for each wavelength, based on the  $\alpha$  Lyrae calibration (Oke and Schild 1970), was derived from observations of four standard stars (HD 19445, 140283, 183143, and 84937) of known absolute-energy distribution. The magnitudes,  $AB$ , at all wavelengths were calculated from the relation  $\log F_v = -0.4AB - 19.438$ , where  $F_v$  is the absolute flux per unit frequency interval.

### *b) Energy Distributions for Virgo Cluster Galaxies from Scanner Data*

We obtained scans for 47 galaxies in the Virgo cluster, and have selected nine of them to illustrate the color-magnitude (C-M) effect by averaging their energy distribution in pairs, where the galaxies have nearly equal apparent magnitudes (ranging from

TABLE 1  
AVERAGE ENERGY DISTRIBUTIONS FOR VIRGO CLUSTER  
GALAXIES MEASURED WITH THE SCANNER\*

$\lambda$ (Å)	$V_{26}$				
	8.7	9.8	10.8	11.8	14.0
	AB Magnitudes				
3466.....	2.92	2.85	2.75	2.64	2.41
3625.....	2.71	2.63	2.53	2.44	2.16
3760.....	2.55	2.44	2.36	2.29	1.92
3970.....	1.85	1.79	1.75	1.69	1.55
4185.....	1.53	1.48	1.44	1.38	1.23
4400.....	1.18	1.15	1.14	1.11	1.00
4618.....	0.92	0.89	0.87	0.84	0.84
4835.....	0.72	0.71	0.72	0.67	0.63
5050.....	0.63	0.63	0.60	0.59	0.56
5378.....	0.45	0.43	0.42	0.43	0.42
5705.....	0.25	0.25	0.25	0.23	0.25
6213.....	0.00	0.00	0.00	0.00	0.00

\* The galaxies that are averaged to obtain the listed values are NGC 4472 and 4486 at  $V_{26} = 8.7$ ; NGC 4526 and 4621 at  $V_{26} = 9.8$ ; NGC 4340 and 4564 at  $V_{26} = 10.8$ ; NGC 4425 and 4377 at  $V_{26} = 11.8$ ; NGC 4328 at  $V_{26} = 14.0$ .

$V_{26} = 8.7$  to 14.0). The resulting mean fluxes are listed in Table 1 and plotted in Figure 1.

The noteworthy features of the diagram are the redder continua for the brightest galaxies, and the progressively increased bluing for fainter galaxies, seen at all wavelengths, but especially strong shortward of  $\lambda 4300$ .

A measure of this wavelength dependence is the magnitude difference,  $\Delta m(\lambda)$ , between the separate curves in Figure 1 at each wavelength, normalized to

$\Delta V_{26} = 1$ . This is the slope  $S(\lambda) \equiv \Delta m(\lambda)/\Delta V_{26}$  of the color-magnitude relation, as read directly from Figure 1, or calculated by least squares from Table 1. The resulting variation of  $S$  with  $\lambda$  is plotted in Figure 2, which shows that the C-M effect increases steadily shortward of  $\lambda 4300$ , and reaches a maximum at the end of our observing range near  $\lambda 3500$ . Figure 2 also shows that  $S(\lambda)$  is nearly zero for  $5000 \lesssim \lambda \lesssim 7000$  Å. This fact will be used in Paper II to derive the galactic reddening from the  $V - r$  colors for the field galaxies, as measured in a discrete-filter color system now to be described.

### III. THE C-M EFFECT FOR THE VIRGO CLUSTER USING AN INTERMEDIATE-BAND $ubVr$ COLOR SYSTEM

#### a) The Color System

When the results of Figure 2 were known, it was evident that photometric observations at discrete wavelengths near  $\lambda(u) \approx 3500$  Å and  $\lambda(V) \approx 5500$  Å alone would maximize the C-M effect, and could be made in a much shorter time per galaxy than could the continuous spectral observations obtained with the scanner. Hence from 1973 May onward all galaxies in the extended program were observed on a simpler four-color system, with discrete filters.

The new system, designated hereafter by  $ubVr$ , was formed by adding two intermediate-band interference filters ( $b$  and  $r$ ) at  $\langle \lambda \rangle = 4522$  Å and  $\langle \lambda \rangle = 6738$  Å (each of total bandwidth of 300 Å) to a standard broad-band  $V$  filter (GG 14 + BG38 with  $\langle \lambda \rangle \approx 5500$  Å,  $\Delta \lambda \approx 800$ ), and retaining the two previous ultraviolet interference filters at  $\langle \lambda \rangle = 3466$  Å and 3625 Å.

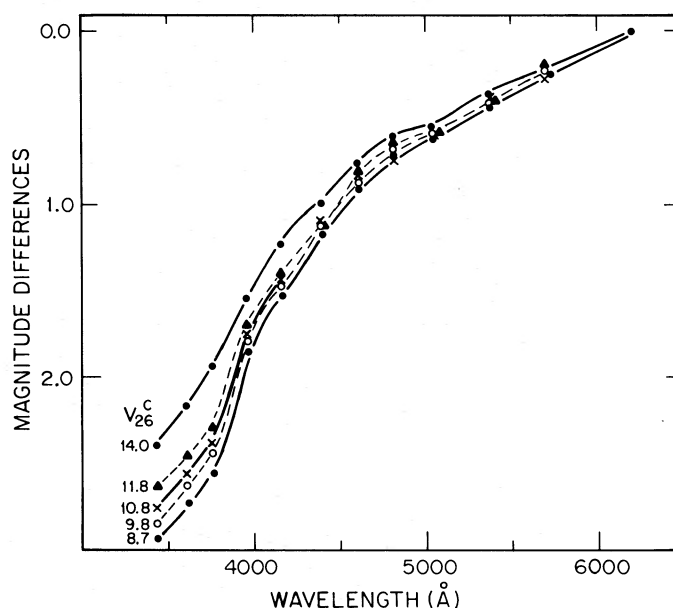


FIG. 1.—Comparison of average energy distributions per unit frequency interval of selected Virgo cluster galaxies of different  $V_{26}$  magnitudes observed with a continuous interference filter and the scanner at a spectral resolution of  $\Delta \lambda/\lambda \approx 0.03$ . The distributions are normalized at  $\lambda 6213$ . The galaxies that have been averaged are listed at the bottom of Table 1.

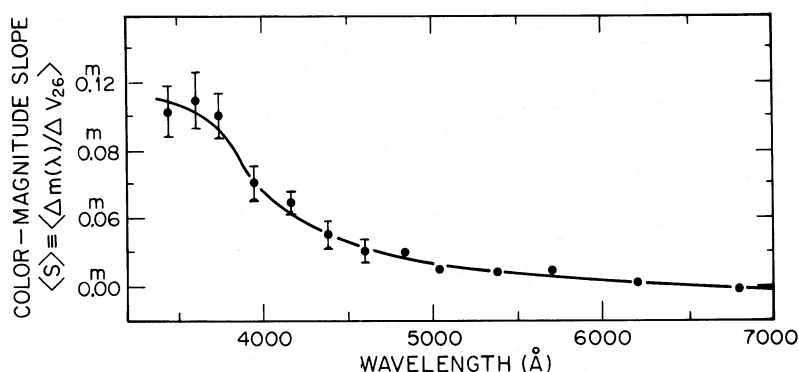


FIG. 2.—Average bluing effect in mag per unit mag difference from the data in Table 1 and Fig. 1

The five filters were mounted in a separate filter wheel that replaced the continuous interference filter, and the scanner was operated as before. In the reductions, we added the flux at  $\lambda\lambda 3466$  and  $3625$  to form a mean point at  $\langle\lambda(u)\rangle \approx 3550$  Å, with effective bandwidth of  $\sim 250$  Å.

The zero-point of the  $V$ -magnitude system was set equal to that of the Johnson and Morgan (1953)  $UBV$  system. The colors  $u - b$ ,  $b - V$ , and  $V - r$  are related to the standard  $U - B$ ,  $B - V$ , and  $V - R$  colors with slope coefficients close to 1.0, but to avoid confusion between the systems we have adopted different color zero points, defined by 12 standard stars whose colors will be given in Paper II.

#### b) The Virgo Cluster $ubVr$ Data

All the scanner data for the 47 Virgo cluster galaxies discussed in §IIb have been reduced to the  $ubVr$  system, using transformations derived from the many galaxies observed in both systems; hereafter in this paper the data will be discussed on this system alone.

Three corrections must be made to the directly observed colors before they can be used to study the C-M relationships. They are (1) correction for color gradients across the face of a given galaxy, depending on the size of the measuring aperture,  $A$ , compared with the reduced galaxy diameter  $D(0)$  (taken from

de Vaucouleurs and de Vaucouleurs [1964]); (2) correction for galactic reddening; and (3) the usual  $K$ -correction to the colors for the effects of redshift.

These corrections, which will be discussed in detail in Paper II, have been applied to all measurements.

The average correction for color gradient from Paper II was applied to each color measured at a particular  $A/D(0)$  aperture ratio, and all corrected observations of a given galaxy were averaged to obtain the color that would have been observed at an interpolated value of  $A/D(0) = 0.5$ .

The correction for reddening was adopted to be a function of galactic latitude alone, by using the idealized cosecant relation of Paper II. This, and the  $K$ -correction corresponding to the systemic velocity, are summarized in Table 2 for the groups and clusters discussed in the present paper. It is to be noted that the  $K(u - V)$  correction is small in the redshift range of these aggregates. The large values for  $K(b - V)$  are due to the fact that the energy distribution curve for E and S0 galaxies has the maximum change of slope near the  $b$  wavelength.

The corrected photometric data for the Virgo galaxies are listed in Tables 3 and 4. In Table 3, the galaxy types in column (2) are new estimates based on large-scale reflector plates from Mount Wilson, Palomar, and Las Campanas. The S0 classification is as described in the *Hubble Atlas*, except that the number added in parentheses denotes the flattening of the

TABLE 2  
CORRECTIONS TO OBSERVED COLORS FOR  $K$  EFFECT AND GALACTIC REDDENING

Cluster (1)	$\langle v \rangle$ ( $\text{km s}^{-1}$ ) (2)	$b^{\text{II}}$ (3)	$K(b - V)$ (mag) (4)	$K(V - r)$ (mag) (5)	$K(u - V)$ (mag) (6)	$E(b - V)$ (mag) (7)	$E(V - r)$ (mag) (8)	$E(u - V)$ (mag) (9)
Virgo.....	1100	$\sim +71^\circ$	0.02	0.00	0.00	0.00	0.00	0.00
Fornax.....	1527	-54	0.02	0.00	0.00	0.00	0.00	0.00
Centaurus.....	3213	+22	0.06	0.00	0.00	0.04	0.04	0.09
Hydra I.....	3450	+26	0.07	0.01	0.00	0.03	0.03	0.07
Pegasus I.....	3836	-48	0.07	0.01	0.00	0.01	0.01	0.02
0122+33.....	5128	-28	0.08	0.01	0.01	0.02	0.03	0.06
Coma.....	6888	+88	0.13	0.02	0.01	0.00	0.00	0.00
CrB.....	21577	+57	0.33	0.04	0.04	0.00	0.00	0.00
Leo.....	926	$\sim +60$	0.00	0.00	0.00	0.00	0.00	0.00
Dorado.....	950	-42	0.00	0.00	0.00	0.01	0.01	0.03

TABLE 3  
E AND S0 CALIBRATORS IN THE VIRGO REGION

NAME	TYPE	$V_{26}^c$	$(b-V)_c$	$(V-r)_c$	$(u-V)_c$	n	AREA
(1)	(2)	(3)	(4)	(5)	(6)	(7)	(8)
NGC 4124*	S0 <sub>3</sub> (6)	11.48	0.45	0.47	2.02	2	< 6°
4179	S0 <sub>1</sub> (9)	10.87	0.57	0.52	2.30	2	> 6°
4262	SB0 <sub>1</sub>	11.40:	0.54	0.54	2.30	0	< 6°
4264	SB0 <sub>2</sub>	12.71	0.44	0.54	2.11	1	> 6°
4267	SB0 <sub>1</sub>	10.80:	0.54	0.55	2.32	1	< 6°
4270	S0 <sub>1</sub> (7)	12.24	0.50	0.50	2.09	1	> 6°
4281	S0 <sub>1</sub> (6)	11.25	0.54	0.55	2.15	1	> 6°
4328	dE	14.06	--	0.47	1.88	2	< 6°
4340	SB0(r)	10.76	(0.54)	(0.47)	(2.17)	1	< 6°
4350	S0 <sub>1</sub> (8)	10.97	(0.45)	0.59	2.25	1	< 6°
4365	E3	9.98	(0.45)	(0.56)	(2.35)	1	< 6°
4371*	SB0 <sub>1</sub> (4)	10.73	0.46	0.58	2.32	1	< 6°
4374	E1 pec	9.37	0.55	0.55	2.40	1	< 6°
4377	S0 <sub>1</sub> (3)	11.73	0.53	0.49	2.11	1	< 6°
4379	E2	11.44	0.50	0.42	2.09	1	< 6°
4382*	S0 <sub>1</sub> (3)	9.28	0.44	0.43	2.07	2	< 6°
4387	E5	12.24	0.49	0.57	2.20	1	< 6°
4406	E2	9.20	0.52	0.47	2.34	3	< 6°
4417	E7/S0(7)	11.32	0.45	0.45	2.15	1	< 6°
4425	S0/Sa:	11.82	0.50	0.37	2.15	1	< 6°
4429	S0 <sub>3</sub> /Sa pec	10.11	0.53	0.58	2.22	1	< 6°
4435	SB0 <sub>1</sub> (7)	10.67	0.52	0.56	2.36	1	< 6°
4442	SB0 <sub>1</sub> (6)	10.32	0.50	0.46	2.25	1	< 6°
4458*	E1	12.01	0.52:	0.53:	2.12:	1	< 6°
4459*	S0 <sub>3</sub> (3)	10.54	0.63:	0.55:	2.29:	1	< 6°
4464*	E3	12.50:	0.52:	0.56:	2.23:	1	< 6°
4468*	E4	12.99	0.51:	0.54:	1.94:	1	< 6°
4472	E2	8.56	0.51	0.51	2.40	2	< 6°
4473	E5	10.28	0.49	0.47	2.30	1	< 6°
4476	E5	12.28	0.47	0.48	2.06	2	< 6°
4477	SB0/SBa	10.23	0.52	0.50	2.34	3	< 6°
4478	E2	11.28	0.48	0.54	2.16	1	< 6°
4479*	SB0	12.57	0.43:	0.57	2.19	1	< 6°
4486	E0	8.79	(0.53)	(0.50)	(2.39)	2	< 6°
4526	S0 <sub>3</sub> (6)/Sa	9.66	(0.51)	(0.55)	(2.26)	1	< 6°
4550	E7/S0	11.31	0.54	0.47	2.17	1	< 6°
4551	E3	11.92	0.42	0.46	2.12	1	< 6°
4552	E0	9.95	0.59	0.52	2.43	4	< 6°
4564	E6/S0 <sub>1</sub>	10.87	0.53	0.52	2.30	1	< 6°
4570	S0 <sub>1</sub> (7)/E7	10.76	0.53	0.53	2.33	1	< 6°
4578	E3	11.15	0.45	0.50	2.14	1	< 6°
4596	SB0/a:	10.47	0.50	0.45	2.20	1	< 6°
4621	E5	9.88	0.52	0.51	2.25	1	< 6°
4623*	E7	12.31	0.51:	0.49:	2.13:	1	< 6°
4636	E0	9.82	(0.39)	(0.67)*	(2.27)	1	> 6°
4638	S0 <sub>1</sub> /E7	11.25	0.49	0.49	2.29	1	< 6°
4649	E2/S <sub>1</sub>	8.90	(0.50)	(0.52)	(2.38)	2	< 6°
4660	E6	10.97	0.55	0.44	2.26	1	< 6°
4754	SB0 <sub>1</sub> (5)	10.40:	0.49	0.52	2.25	1	> 6°
4762	S0 <sub>1</sub> (10)	10.38	0.53	0.46	2.13	1	> 6°

\*Not used in the solutions. Plotted as + in Figure 3.

( ) are values where the color-aperture correction is large.

TABLE 4  
FAINT VIRGO CLUSTER CALIBRATORS MEASURED PREVIOUSLY

Name*	Other	Type	$V_{26}^c$	$(b-V)_c^\dagger$	$(u-V)_c^\dagger$
M100, 1.....	IC 783	dE	14.5	0.43	1.85
M100, 2.....	...	dE	16.5	0.39	1.69
M100, 3.....	IC 783A	dE	16.0	0.43	1.74
M100, 4.....	N4322	dE	15.0	0.45	1.96
M100, 5.....	N4328	dE	14.06	0.47	1.88
M100, 6 <sub>‡</sub> .....	...	dE	17.0	0.18	1.24

\* The numbers for the M100 dwarfs given here are the same as in Table 2 of Sandage (1972a). Some of the markings on the chart in that paper are incorrect and should be, in order of the Table 2 values, 2, 6, 3 (same), 4 (same), 1, and 5.

† The colors listed here were transformed from the *UBV* system in which they were measured to the present system by equations in the forthcoming Paper II.

‡ M100, 6 was not used in the least-squares solutions.

galaxy, as used for E systems. The magnitude  $V_{26}$  in column (3) is the same as defined for the southern hemisphere galaxy photometry (Sandage 1975), as explained more fully in Paper II. The external accuracy of the listed values is believed to be  $\sigma(V_{26}) \approx \pm 0.1$  mag. (The corrections to  $V_{26}$  for galactic reddening and for  $K$  dimming are adopted to be zero for Virgo cluster galaxies.) Columns (4)–(6) list the colors  $(b - V)_{0.5}$ ,  $(V - r)_{0.5}$ , and  $(u - V)_{0.5}$  as reduced to  $A/D(0) = 0.5$ , again corrected for  $K$ -term and reddening, which again are assumed to be zero in Virgo, except for  $K(b - V)$ . Column (7) gives the number of observations that go into the means of columns (4)–(6). Column (8) indicates whether the galaxy is inside or outside the central  $6^\circ$  (radius) region of the cluster center, taken to be at  $\alpha(50) = 12^h 25^m$ ,  $\delta(50) = +13^\circ 06'$ . The nine galaxies marked with asterisks in column (1) were not used in the least-squares solutions that follow, because they either stand far from the mean C-M relations or have high observational errors (i.e.,  $\geq \pm 0.03$  mag) in the colors owing to insufficient photon statistics, for reasons of short exposure times. The photon statistics of all other entries is generally smaller than  $\pm 0.02$  mag, and in most cases  $\pm 0.01$  mag. (The detailed individual observations that have been used to derive the

corrected mean values in Table 3 will be listed and discussed in Paper II.)

Because dwarf E galaxies fainter than  $V = 14$  in the Virgo cluster could not be observed effectively with the Palomar 1.5 m telescope, we have converted the previously available  $UBV$  data from the Hale 5 m reflector (Sandage 1972a) to the present  $ubVr$  system for six such galaxies, with the results listed in Table 4. Although the  $u - V$  colors have uncertainties as high as  $\pm 0.05$  mag due to the transformations, we have used them in the next section to extend the C-M relations for Virgo E and S0 galaxies to faint limits.

### c) The Color-Magnitude Effect for Virgo Cluster Galaxies

The data from Tables 3 and 4 for Virgo cluster galaxies alone are plotted in the color-magnitude diagram of Figure 3. Closed circles are E and S0 galaxies within  $6^\circ$  of the adopted cluster center, crosses are galaxies with  $r > 6^\circ$ , vertical crosses are the galaxies marked with asterisks in Table 3 (not used in the solutions), and open circles are from Table 4.

The change in  $(u - V)_c$  with  $V_{26}$  is pronounced and well defined, ranging from  $(u - V)_c = 2.5$  to  $(u - V)_c = 1.7$  mag as  $V_{26}$  varies from 8 to 16 mag.

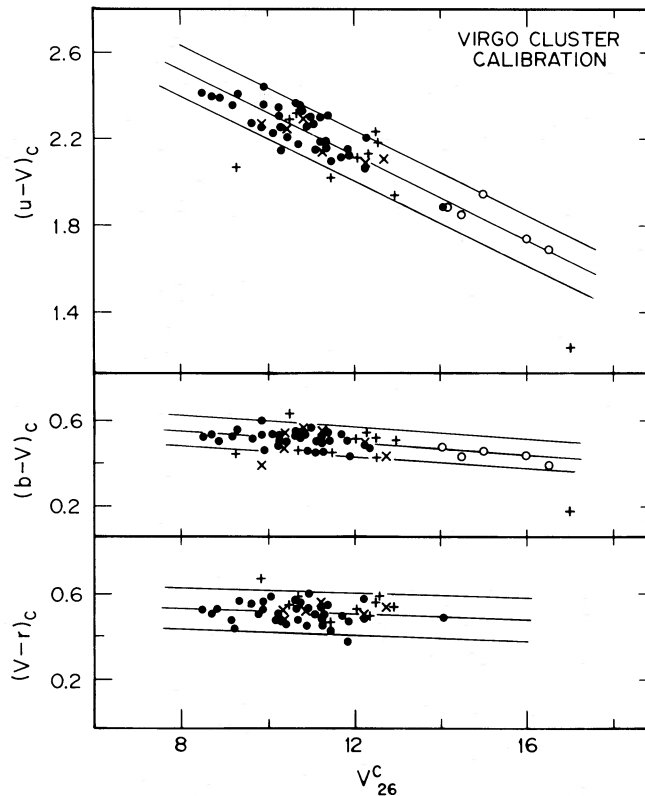


FIG. 3.—The color-magnitude effect for Virgo cluster galaxies listed in Tables 3 and 4. Dots, galaxies within  $6^\circ$  of the cluster center. Diagonal crosses have  $r > 6^\circ$ ; open circles are transformed to the  $ubV$  color system from  $UBV$  literature values; vertical crosses were not used in the least-squares solutions. Heavy lines, eqs. (1)–(3) of the text. Boundary lines are at  $\pm 2\sigma$  of the color residuals.

TABLE 5  
OTHER CLUSTER CALIBRATORS

NAME	TYPE	$V_{26}^c$	$(b-V)_c$	$(V-r)_c$	$(u-V)_c$	n
(1)	(2)	(3)	(4)	(5)	(6)	(7)
FORNAX						
N 1316	E4 pec	8.67	0.52	0.54	2.37	3
1316c	-	13.00	0.46	0.47	2.01	2
1351	SO <sub>1</sub> (6)/E6	11.78	0.50	0.51	2.17	2
1374	E0 <sup>†</sup>	11.48	0.54	0.49	2.32	3
1375	SO <sub>1</sub> (5)	12.67	0.41	0.48	1.96	1
1379	E0	11.26	0.53	0.45	2.24	2
1380B	E4	13.00	0.53	0.45	2.12	2
1380	SO (7)	9.99	0.53	0.51	2.30	2
1381	SO <sub>1</sub> (9)	11.35	0.56	0.46	2.25	3
1386	SO <sub>1</sub> (7)	11.07	0.51	0.51	2.15	3
1387	SB0	10.76	0.61	0.56	2.39	4
1389	SO <sub>1</sub> (4)/E4	11.47	0.56	0.46	2.20	1
1399	E1	9.89	0.56	0.48	2.41	2
1404	E2	10.06	0.57	0.51	2.40	5
1427	E5	11.12	0.55	0.47	2.17	3
CENTAURUS						
4645	E5	11.62	0.60	0.60	2.48	1
4696	E3	10.27	0.59	0.62	2.47	1
4767	E5	11.49	0.60	0.54	2.42	1
IC 3370	E2	11.03	0.53	0.55	2.44	1
HYDRA I (ABELL 1060)						
N 3309	E1	11.56	0.52	0.52	2.44	1
PEGASUS 1						
N 7562	E2	11.79	0.55	0.58	2.38	1
7617	E6	13.89	0.54	0.70	2.11	1
7619	E3	11.25	0.60	0.55	2.56	1
7626	E1	11.22	0.55	0.57	2.48	2
0122 + 3305						
N 499	E5	11.98	0.58	0.55	2.52	1
507	SO <sub>1</sub> (3)	11.60	0.56	0.54	2.46	1
508	E0	12.69	0.66	0.62	2.36	1
COMA						
N 4860	E	13.45	0.57	0.50	2.40	2
4873	SO	14.25	0.55	0.48	2.31	2
4874	SO	12.59	0.61	0.52	2.47	3
RB 37	SO	16.80	0.48	0.47	1.95	1
42	SO	15.76	0.53	0.53	2.21	1
IC 3998	SB0	14.60	0.63	0.55	2.37	1
N 4881	E0	13.58	0.49	0.49	2.31	2
4883	SB0	14.21	0.54	0.53	2.33	1
4886	E0	13.97	0.53	0.54	2.29	1
IC 4011	E0	15.06	0.48	0.49	2.09	1
IC 4012	E3	14.95	0.53	0.50	2.18	1
N 4889	E4	11.72	0.51	0.52	2.43	5
IC 4026	SB0	14.76	0.53	0.51	2.24	1
IC 4042	SB0	14.37	0.52	0.49	2.25	1
N 4923	E0	13.81	0.53	0.53	2.33	1
CORONA BOREALIS						
# 2	E	14.84	0.61	0.48	2.59	1
3	E	15.95	0.66	0.53	2.49	1
8	E	15.15	0.58	0.48	2.45	2

The change in  $(b - V)_c$  and  $(V - r)_c$  is much less, in agreement with Figure 2. The slopes of the C-M relations in the different colors can be read in an obvious way from Figure 2 as  $\Delta(u - V)_c/\Delta V_{26} \approx 0.10$  mag/mag,  $\Delta(b - V)_c/\Delta V_{26} \approx 0.02$  mag/mag, and  $\Delta(V - r)_c/\Delta V_{26} \approx 0.01$  mag/mag, which are satisfactorily close to the actual slopes in Figure 3 that follow from the complete material and the following calculation.

Formal least-squares solutions from Tables 3 and 4 (alternately taking  $V_{26}$  and the color as the independent variable and averaging the two regressions for the  $u - V$  solution) give

$$(u - V)_c = -0.0968V_{26} + 3.28, \quad n = 46, \quad (1)$$

$$(b - V)_c = -0.0144V_{26} + 0.658, \quad n = 45, \quad (2)$$

$$(V - r)_c = -0.0079V_{26} + 0.589, \quad n = 40, \quad (3)$$

where the correlation coefficients of equations (1)–(3) are 0.92, 0.55, and 0.19, respectively.

It is to be emphasized that the values of the slopes and intercepts of these equations are quite sensitive to (1) the transformed  $ubV$  values for the five faint dwarf E galaxies from Table 4, which, as previously stated, have uncertainties of  $\sim \pm 0.05$  mag in  $(u - V)_c$  and  $(b - V)_c$ , and (2) unknown biases due to the obvious incompleteness of the sample at all magnitudes (the areas between the  $\pm 2\sigma$  lines in Fig. 3 are not uniformly filled). Hence, although the least-squares solutions have been made, their significance is more a formality than a necessarily precise statement of the regressions.

Nevertheless, we adopt equation (1) as the best description of the C-M correlation in Virgo from the

current material, and use it in the tests for universality set out in the next sections.

One should note here that the galaxies plotted as crosses in Figure 3 are those more distant than  $6^\circ$  from the Virgo cluster center. The good agreement of the crosses with the mean regressions shows that most of these outlying galaxies are at the same mean distance as those closer to the center, and hence that the true radius of the Virgo cluster is larger than  $r = 6^\circ$ .

#### IV. COLOR-MAGNITUDE EFFECT IN EIGHT NEARBY GROUPS AND CLUSTERS

To test the universality of the C-M effect, we obtained data for galaxies in a number of groups and clusters in the Shapley-Ames catalog, and a few fainter systems.

The color-magnitude data for seven clusters, corrected for  $K$ -term, reddening, and color-aperture gradients, as described earlier, are listed in Table 5. Similar data for the two nearby groups in Leo and Dorado are given in Table 6. The observations in Coma and Corona Borealis were made with the Hale 5 m reflector, and the others with the Swope 1 m reflector at Las Campanas, or the 1.5 m telescope at Palomar.

The C-M effect for both the Fornax and Coma clusters is well defined, as the reader can verify by plotting the listed data. Least-squares regressions of the colors on  $V_{26}^c$  for the two clusters are given in Table 7. The slopes for both are nearly identical with those for Virgo (eqs. [1]–[3]). In addition, the zero-point shifts in magnitudes,  $\Delta(m - M)_0$ , are close to  $\Delta \log v \equiv 5 \log v/v_{\text{VIRGO}}$ , which is the requirement for the same absolute magnitude for a given color, provided that the velocity field is Hubble-like.

TABLE 6  
LEO AND DORADO GROUPS

Name (NGC No.) (1)	Type (2)	$V_{26}^c$ (3)	$(b - V)_c$ (4)	$(V - r)_c$ (5)	$(u - V)_c$ (6)
Leo					
3377.....	E6	10.34	0.52	0.49	2.17
3379.....	E0	9.60	0.58	0.51	2.40
3384.....	SB0 <sub>1</sub> (5)	9.58:	0.54	0.50	2.32
3412.....	SB0 <sub>1/2</sub>	10.54:	0.54	0.46	2.17
3489.....	S0 <sub>3</sub> (5) or SBa	10.20	0.52	0.45	2.10
3607.....	S0 <sub>3</sub> (3)	10.11	0.57	0.52	2.36
3608.....	E1	11.02	0.58	0.49	2.34
3626.....	S0 <sub>3</sub> (4)	10.88	0.50	0.46	2.12
Dorado					
1533.....	E4/S0 <sub>1</sub> (4)	10.60	0.57	0.51	2.31
1543.....	RSBO	10.33	0.56	0.49	2.31
1546.....	[S0 <sub>1</sub> (7)]:	11.42	0.57	0.60	2.04
1549.....	E2	9.81	0.54	0.45	2.25
1553.....	S0 <sub>1</sub> (5)	9.31	0.59	0.47	2.32
1574.....	E4	10.29	0.53	0.50	2.31
1596.....	S0 <sub>1</sub> (8)	11.10	0.57	0.42	2.29
1617.....	Sa(s)	10.28	0.54	0.56	2.29

TABLE 7  
COMPARISON OF THE INDIVIDUAL REGRESSIONS FOR THE  
FORNAX, COMA, AND VIRGO CLUSTERS

Parameter	Fornax	Coma	Virgo
$(u - V)_c$ versus $V_{26}^c$			
Slope (mag/mag).....	-0.10	-0.10	-0.10
	$\pm 0.01$	$\pm 0.01$	$\pm 0.01$
$\sigma(u - V)_c$ (mag).....	$\pm 0.07$	$\pm 0.06$	$\pm 0.06$
$n$ .....	+15	+15	+46
$r$ .....	+0.85	+0.91	+0.92
$(b - V)_c$ versus $V_{26}^c$			
Slope (mag/mag).....	-0.02	-0.01	-0.02
	$\pm 0.01$	$\pm 0.01$	$\pm 0.01$
$\sigma(b - V)_c$ (mag).....	$\pm 0.04$	$\pm 0.03$	$\pm 0.03$
$n$ .....	+15	+15	+15
$r$ .....	+0.43	+0.43	+0.72
$(V - r)_c$ versus $V_{26}^c$			
Slope (mag/mag).....	-0.02	-0.01	-0.01
	$\pm 0.01$	$\pm 0.01$	$\pm 0.01$
$\sigma(V - r)_c$ (mag).....	$\pm 0.03$	$\pm 0.02$	$\pm 0.04$
$n$ .....	+15	+15	+40
$r$ .....	+0.65	+0.59	+0.23
Differences in Photometric and Redshift Moduli Relative to Virgo			
$\Delta(m - M)_0$ .....	+0.32	+3.89	0.00
	$\pm 0.23$	$\pm 0.20$	
$5 \log(v/v_{\text{VIRGO}})$ .....	+0.71	+3.98	0.00
	$\pm 0.20$	$\pm 0.14$	

In Table 7, where the entries are generally self-explanatory, the symbol  $n$  is the number of observations and  $r$  is the correlation coefficient of each regression. The last entries show the difference in zero point,  $\Delta(m - M)_0$ , calculated from the C-M data, compared with the expected magnitude shift if the ratio of the redshifts (given later in Table 8) is the ratio of the distance.

We have made a further test of universality by combining the material for the clusters and groups from Tables 5 and 6 by shifting the observed  $V_{26}^c$  magnitudes for each aggregate to the Virgo cluster distance by  $\Delta V_{26}^c = 5 \log v/v_{\text{VIRGO}}$ . The results, given in Figure 4, show that the regression lines, copied from Figure 3 for Virgo, fit the plotted points well. This clearly supports the case for universality. Furthermore, the dispersions about the ridge line are nearly the same as for the Virgo cluster itself. These agreements are particularly striking when we keep in mind that the eight groups and clusters that form the composite C-M diagrams of Figure 4 are of different richness and Bautz-Morgan types. This, together with the demonstration in Paper II that the C-M correlation also applies to galaxies in the *general field*, emphasizes that the phenomenon, whatever its cause, is not affected by the environment in which particular galaxies find themselves.

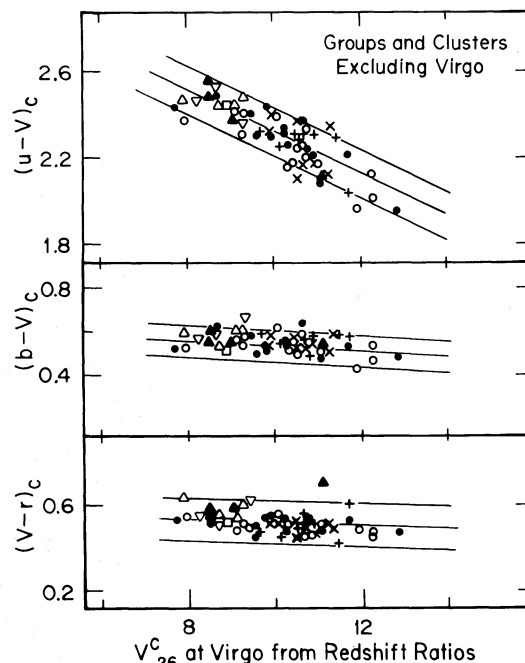


FIG. 4.—The C-M effect for clusters and groups, reduced to the Virgo cluster distance by magnitude shifts of  $\Delta V_{26}^c = 5 \log v/v(\text{Virgo})$ . The colors are corrected for color-aperture gradient, and for  $K$ -term and galactic reddening, where appropriate. The coding is diagonal crosses for Leo, vertical crosses for Dorado, open circles for Fornax, open triangles for Centaurus, open square for Hydra I, closed triangles for Pegasus I, closed dots for Coma, and inverted triangles for 0122+33. The lines are the same as in Fig. 3 for Virgo alone.

The agreement between the separate C-M diagrams is emphasized again in Figure 5, where the  $(u - V)_c$ ,  $V_{26}^c$  pairs for the cluster and group galaxies are combined with Virgo directly, again by shifts from the ratio of redshifts. As before, the comparison is quite satisfactory, from which we conclude that a common

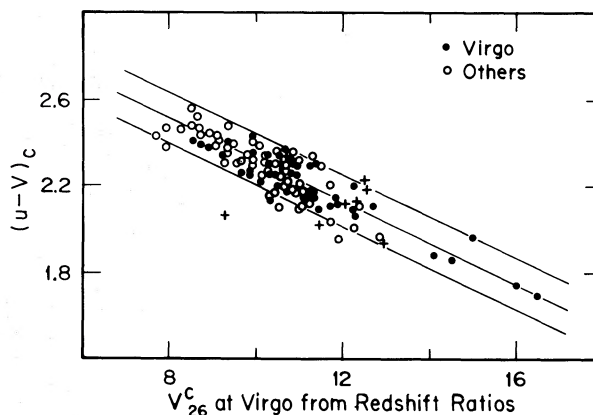


FIG. 5.—Composite C-M diagram in  $(u - V)_c$  for data in Tables 3–5, brought to the Virgo cluster distance by magnitude differences related to the ratio of the redshifts. Coding separates Virgo cluster galaxies from galaxies in all other groups and clusters. Vertical crosses, Virgo galaxies not used in the solution. The lines are the same as in Fig. 3.

TABLE 8  
DISTANCE MODULI FOR EIGHT CLUSTERS AND GROUPS SHIFTED TO THE VIRGO CLUSTER (assumed at  $m - M = 31.70$ )  
BY FORCING COINCIDENCE OF THE COLOR-MAGNITUDE RELATIONS

Name (1)	$n$ (2)	$(m - M)_0$ (mag) (3)	$v_0$ ( $\text{km s}^{-1}$ ) (4)	$\Delta(m - M)$ (mag) (5)	$5 \log (v/v_{\text{VIRGO}})$ (mag) (6)
Virgo.....	46	$31.70 \pm 0.08$	$1100 \pm 68$	0.00	0.00
Leo.....	8	$31.30 \pm 0.42$	$926 \pm \sim 100$	$-0.40 \pm 0.43$	$-0.37 \pm 0.27$
Dorado.....	8	$31.59 \pm 0.29$	$935 \pm \sim 100$	$-0.11 \pm 0.30$	$-0.35 \pm 0.27$
Fornax.....	15	$32.02 \pm 0.21$	$1527 \pm \sim 100$	$+0.32 \pm 0.23$	$+0.71 \pm 0.20$
Centaurus.....	4	$34.24 \pm 0.35$	$3170 \pm \sim 50$	$+2.54 \pm 0.36$	$+2.30 \pm 0.14$
Hydra I.....	1	$34.57 \pm \sim 0.5$	$3697 \pm 284$	$+2.87 \pm \sim 0.5$	$+2.63 \pm 0.21$
Pegasus I.....	4	$34.45 \pm 0.49$	$3836 \pm 127$	$+2.75 \pm 0.50$	$+2.71 \pm 0.15$
0122+33.....	3	$35.17 \pm 0.40$	$5128 \pm \sim 100$	$+3.47 \pm 0.41$	$+3.34 \pm 0.14$
Coma.....	15	$35.59 \pm 0.18$	$6888 \pm 68^*$	$+3.89 \pm 0.20$	$+3.98 \pm 0.14$

\*  $\langle v \rangle$  for Coma from Rood *et al.* (1972).

color-magnitude effect applies to all groups in our sample.

However, the nonuniform distribution of points in Figures 4 and 5 fainter than  $V_{26}^c \approx 11$  show that this sample, like that for Virgo alone, is quite incomplete. Hence it would be incorrect to calculate new regressions for the entire material in an effort to improve equations (1)–(3). Because of this bias, we have adopted the slope of the equations from the Virgo cluster itself for the remainder of the paper.

#### V. THE VELOCITY-DISTANCE RELATION FROM THE COLOR-MAGNITUDE EFFECT

Detailed inspection of Figures 4 and 5 shows that slight systematic differences exist between several of

the clusters in the composite C-M diagram when the shifts in  $V_{26}^c$  are made by the ratio of the redshifts. We therefore ask for the individual shifts,  $\Delta V_{26}^c$ , that will give *minimum* scatter in a composite C-M diagram, and further ask for the correlation of these  $\Delta V_{26}^c$  values with redshift as a test of the local velocity field.

The shifts for minimum scatter were computed by least squares from data in Tables 5 and 6, using the slope  $\Delta(u - V)_c / \Delta V_{26}^c = -0.0968$  from equation (1). The results, given in column (5) of Table 8, represent the best values for the difference in distance modulus between each group and the Virgo cluster, based solely on the color-magnitude effect. They are, in effect, photometric parallaxes of the aggregates. Hence, by adopting the modulus of Virgo to be  $(m - M)_0 = 31.70$  (Sandage and Tammann 1976b), we find the

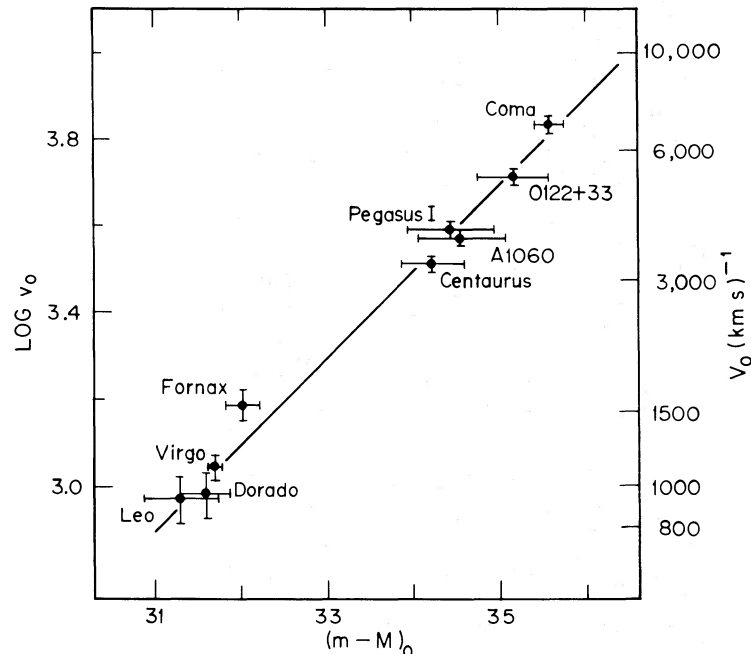


FIG. 6.—Velocity-distance relation using photometric parallaxes for the eight clusters and groups from Table 8 and an assumed modulus of  $(m - M)_0 = 31.70$  for the Virgo cluster. The distant CrB cluster from Table 5 is not plotted, as we are concerned here only with the local velocity field. A line of slope 5, corresponding to a linear velocity-distance relation, is assumed.

moduli for each group or cluster by adding column (5) to 31.70, with the result listed in column (3) of Table 8.

The systemic velocities in Table 8 are taken from Rood *et al.* (1972) for Coma, from Sandage and Tammann (1976a) for Virgo, and from Sandage (1975) for the remainder. The observed velocities have been corrected for a solar motion relative to the assumed inertial frame of  $300 \sin l \cos b \text{ km s}^{-1}$ .

The resulting velocity-distance relation for  $v_0 \lesssim 7000 \text{ km s}^{-1}$  is shown in Figure 6, where a line of slope 5 is assumed, and the fit is made for zero mean deviation of the points, giving

$$(m - M)_0 = 5 \log v_0 + 16.535 (\pm 0.073). \quad (4)$$

The dispersion about the mean line is  $\sigma(m - M) = \pm 0.21 \text{ mag}$ , using all the data.

Figure 6 can be interpreted in two ways. (1) If we assume that the C-M effect has the same zero point in absolute magnitude from cluster to cluster, then Figure 6 shows again that the velocity-distance relation is closely linear for local clusters. In this regard, the good agreement of the Virgo cluster with the mean line demonstrates the lack of measurable velocity perturbation at the Virgo cluster relative to the mean velocity field of the remaining clusters, at a level of  $\Delta v \approx \pm 25 \text{ km s}^{-1}$ , which is within a  $0.3 \sigma$  spread of the uncertainty in the Virgo cluster velocity itself. (2) On the other hand, if we adopt the premise that the local velocity-distance relation is in fact linear, as suggested by previous work (Sandage 1972b; Sandage and Hardy 1973; Sandage 1975), then Figure 6 demonstrates that the absolute-magnitude calibration of the C-M effect is the same from cluster to cluster.

We should also note that the difference in photometric distance moduli [ $\Delta(m - M)$  in Table 8] between Coma and Virgo is  $\Delta V_{26}^c = 3.89 \pm 0.20$ . This does not support a difference of 4.7 mag required by Abell and Eastmond (1968) or by Abell (1972), based on the assumption that apparent breaks in the luminosity functions occur at a particular absolute magnitude.

Finally, it should be noted that equation (4) leads to a Hubble constant of  $H_0 = 49.3 \pm 1.6 \text{ km s}^{-1} \text{ Mpc}^{-1}$ , but the value depends on the assumption of  $(m - M)_0 = 31.70$  for the Virgo cluster itself. Because equation (4) is based on only nine local clusters and groups, this value of  $H_0$  has rather low weight, despite the small formal error.

#### VI. INTRINSIC SCATTER IN THE C-M DIAGRAMS

It is now of interest to compare the scatter in Figure 3 with the known observational errors to test whether the cosmic dispersion of the C-M effect has been reached, or whether we could expect decreased scatter with more accurate observations. The color residuals from the Virgo cluster correlations alone (Fig. 3) are distributed with  $\sigma(u - V)_c = \pm 0.059 \text{ mag}$ ,  $\sigma(b - V)_c = \pm 0.035 \text{ mag}$ , and  $\sigma(V - r)_c = \pm 0.046 \text{ mag}$ .

The errors of observation contribute part of the scatter and are of order  $\pm 0.03 \text{ mag}$  in all colors. Hence the color residuals in  $(b - V)_c$  and  $(V - r)_c$

are mostly due to these errors. However, there is an excess scatter of  $[(0.059)^2 - (0.03)^2]^{1/2} = 0.05 \text{ mag}$  in  $\sigma(u - V)_c$  which cannot be accounted for in this way.

The  $\sigma(u - V)_c$  excess can be caused by a combination of (1) errors in  $V_{26}^c$ ; (2) the mixing of E and S0 galaxies in the C-M diagrams if the effect is different for the two types; (3) possible patchy reddening within the clusters; and (4) a true cosmic scatter for reasons intrinsic to the unknown physics of the C-M effect itself.

The observational error in  $V_{26}^c$  is of order  $\sigma(V_{26}^c) = \pm 0.1 \text{ mag}$ . Furthermore, the assumption that all Virgo cluster galaxies are at the same distance gives a spread of  $\pm 0.23 \text{ mag}$  in  $V_{26}^c$  due to the back-to-front ratio over the cluster area of radius  $6^\circ$ . The scatter introduced by these combined errors corresponds to  $\sigma(V_{26}^c) = \pm 0.25$ , or only  $\sigma(u - V)_c = \pm 0.025 \text{ mag}$ , from equation (1).

The difference in the color-magnitude effect for E and S0 galaxies has been investigated by fitting least-squares linear relations to the galaxy types separately in Figures 3–5. The scatter in  $(u - V)_c$  for E galaxies is found to be  $\sigma(u - V)_c = \pm 0.057 \text{ mag}$ , and  $\sigma(u - V)_c = \pm 0.063$  for S0 systems, which are nearly the same as we found above for E and S0's taken together. Furthermore, the zero points of the C-M relations are the same for the E and S0 galaxies, as shown in Figure 7, where the galaxies from the nine groups and clusters are combined by using the minimum deviation shifts (i.e., the photometric parallaxes) from Table 8. The E and S0 galaxies commingle in the diagrams, with no evident difference in either slope or zero point. This similarity of the color distributions for E and S0 systems within their common C-M correlation is one of the principal results of this paper.

The case for something peculiar within the clusters themselves, such as patchy reddening by intercluster dust, also finds no support from the present data. If a Whitford-like reddening law were involved, one would expect  $\sigma(u - V)_c \approx 1.7\sigma(u - b)_c$ , which can be shown not to occur with the present data. Furthermore, we show in Paper II that the *field* galaxies also have the same large  $\sigma(u - V)_c$  dispersion, a circumstance that excludes all explanations that rely on special conditions within clusters.

Hence, because neither errors in  $V_{26}^c$ , nor differences between E and S0 galaxies, nor internal reddening contributes significantly to the excess  $\sigma(u - V)_c$  value, we conclude that most of the scatter in this color is intrinsic to the C-M effect itself.

#### VII. ABSOLUTE CALIBRATION AND EXPECTED ACCURACY OF INDIVIDUAL PHOTOMETRIC PARALLAXES

From the tests described in §§ IV and V, we conclude that the same color-magnitude effect applies to various groups and clusters. Furthermore, it applies equally to E and S0 galaxies. Hence, once the relation has been absolutely calibrated, it is possible to obtain therefrom photometric distance moduli for individual E and S0 galaxies in clusters, in groups, and presumably in the general field.

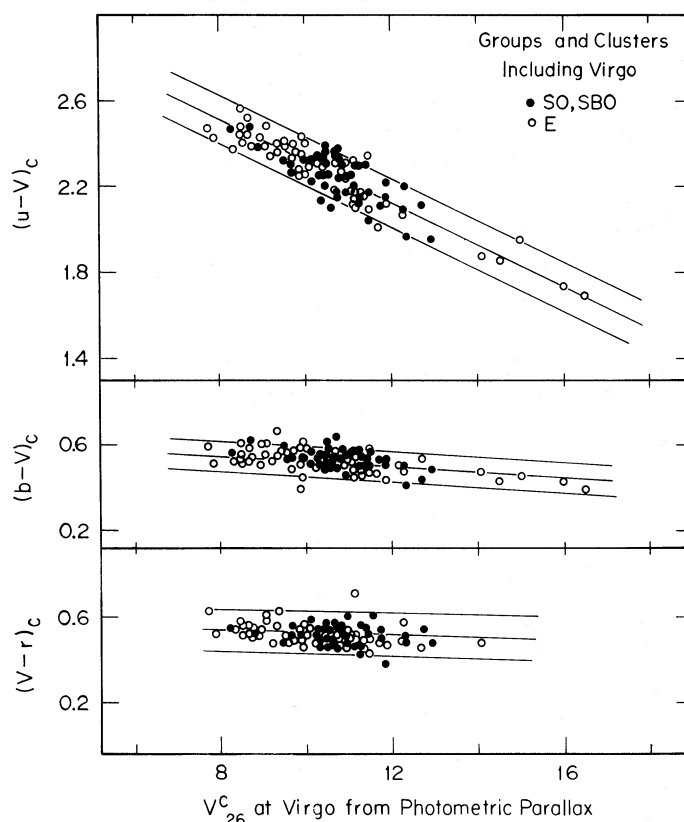


FIG. 7.—Composite C-M diagram for all galaxies in the sample, shifted to the Virgo cluster distance by magnitude differences calculated from the photometric parallaxes. Galaxies of E and S0 types are shown with different symbols. The ridge line is the Virgo cluster solution of Fig. 3. Boundary lines are at  $\pm 2\sigma$  in the color residuals.

If we adopt equation (1) as the best description of the shape of the correlation, and also assume  $(m - M)_0 = 31.70$  for Virgo as before, then the absolute calibration becomes

$$M_{V_{26}^c} = -10.327(u - V)_c + 2.19. \quad (5)$$

The individual accuracy for an absolute magnitude of a single E or S0 galaxy depends upon the cosmic scatter of  $(u - V)_c$ , which from the last section is  $\sigma(u - V)_c \approx 0.05$  mag, giving  $\sigma(M) = \pm 0.5$  mag. This accuracy, which is closely the same as for the highest luminosity spirals (Sc I, Sc I-II, Sc II) using the van den Bergh luminosity classes, permits distances to single E and S0 galaxies to be determined to within  $\sigma(\delta r/r) = \pm 0.22$ . This is accurate enough to make feasible an attempt to measure the local velocity field by using these types of galaxies.

#### VIII. DISCUSSION AND CONCLUSIONS

To this point we have been concerned solely with the astronomical aspects of the color-magnitude relation, showing that it is the same in all aggregates studied here, and that it can be used to find relative distances. But of more fundamental interest is the reason why the blueness of the stellar content (i.e., of the composite

H-R diagram) is connected with the total luminosity, and hence to the mass of the E or S0 galaxy, and why this connection is so regular from galaxy to galaxy.

It would not, of course, be so surprising to find that a series of chemical enrichments and subsequent star formations have occurred in individual galaxies so as to give rise to a particular state of the stellar content (i.e., with a particular H-R diagram), and hence a particular integrated color. But what is so unexpected is that the rate of the process depends so *tightly* and so universally on the mass of the parent galaxy.

The problem can be divided into two parts, both of which are currently unsolved. (1) What is the composite H-R diagram of the stellar content for the galaxies in Figures 3-7, and what are the parameters that change progressively as we move along these C-M regression lines? (2) Why do these parameters vary in such a regular way with the galactic mass?

It seems clear that *age* is not a parameter because at least some of the galaxies in our sample are in clusters, precluding that possibility, since all galaxies in a given cluster are presumably coeval. Faber's (1973) study of absorption-line equivalent widths suggests that the principal parameter is average metal abundance; hence a first attempt at modeling would be to construct composite H-R diagrams with different metal

abundances to test the integrated colors. At the moment, this particular approach appears tractable because of two developments.

a) The near-infrared observations of Frogel and Persson (1977) of Virgo cluster galaxies show that the C-M effect *again becomes pronounced for*  $V - K$  ( $K$  at  $2.2 \mu\text{m}$ ) colors, in the sense that  $V - K$  is bluer for intrinsically fainter galaxies. Thus Figure 1, if extended to  $2.2 \mu\text{m}$ , would show the energy-distribution curves separating again at longer wavelengths. This observation is a crucial constraint on proper modeling of the composite H-R diagram as a function of galaxy luminosity, and, together with the  $UV$  and near-red observations here, may be enough to define the problem broadly.

b) The large grid of isochrones and theoretical luminosity functions for a wide range of chemical compositions and ages, computed by Ciardullo and Demarque (1977) from evolutionary tracks by Mengel *et al.* (1977), provide the necessary theoretical apparatus to explore the integrated colors of various composite H-R diagrams. When these tracks are folded into the variable blanketing effect of Fraunhofer lines of different strengths, and weighted by proper luminosity functions, we might expect to understand the stellar contents (of different metal abundances) that could give rise to the C-M effect of Figures 1–5.

However, the more fundamental question remains of why the parameters, whatever they are, vary in step with the galactic mass. Provided that we can reach an understanding of the first problem—which parameters vary—there is a chance that an answer to the second question of the mechanism can be found.

For example, if one could show that the variable parameter *is* metal abundance alone, then it would seem relatively easy to prescribe the controlled events of a metal-enrichment rate as a function of total mass (via supernovae rates, to name but one). However, until the forms of the composite H-R diagrams are known, an answer to the second question—the nature of the cause—will remain only a set of possibilities.

This work was supported by a grant from the National Science Foundation MPS 72-05099 and by special funds from the Carnegie Institution of Washington, for which we are grateful. It is also a pleasure to thank the night assistants, Antoine Guerra at Las Campanas, and the late Dennis Palm at Palomar, and the maintenance crews on both mountains for special help during the three years of the observations. Special thanks go to Gomathi Visvanathan for her help in the programming and in the reduction of the data in a critical period of the project.

#### REFERENCES

- Abell, G. 1972, in *IAU Symposium No. 44, External Galaxies and Quasi-Stellar Objects*, ed. D. S. Evans (Dordrecht: Reidel), p. 341.
- Abell, G., and Eastmond, S. 1968, *A.J.*, **73**, S161.
- Baum, W. A. 1959, *Pub. A.S.P.*, **71**, 106.
- Ciardullo, R. B., and Demarque, P. 1977, *Yale Transactions*, vols. **33**, **34**, and **35**.
- Code, A. D. 1959, *Pub. A.S.P.*, **71**, 118.
- de Vaucouleurs, G. 1958, *A.J.*, **63**, 253.
- . 1961, *Ap. J. Suppl.*, **5**, 233.
- . 1976, *Ap. J.*, **205**, 13.
- de Vaucouleurs, G., and de Vaucouleurs, A. 1964, *Reference Catalogue of Bright Galaxies* (Austin: University of Texas Press).
- . 1972, *Mem. R.A.S.*, **77**, 1.
- Faber, S. M. 1973, *Ap. J.*, **179**, 731.
- Frogel, J., and Persson, E. 1977, private communication.
- Johnson, H. L., and Morgan, W. W. 1953, *Ap. J.*, **117**, 313.
- Lasker, B. M. 1970, *A.J.*, **75**, 21.
- McClure, R. D., and van den Bergh, S. 1968, *A.J.*, **73**, 1008.
- Mengel, J. G., Sweigart, A. V., Demarque, P., and Gross, P. G. 1977, *Ap. J. Suppl.*, in press.
- Oke, J. B., and Schild, R. 1970, *Ap. J.*, **161**, 1015.
- Peebles, P. J. E. 1976, *Ap. J.*, **205**, 318.
- Rood, H. J. 1969, *Ap. J.*, **158**, 657.
- Rood, H., Page, T., Kintner, E., and King, I. 1972, *Ap. J.*, **175**, 627.
- Rubin, V. C., Thonnard, N., Ford, W. K., and Roberts, M. S. 1976, *A.J.*, **81**, 719.
- Sandage, A. 1972a, *Ap. J.*, **176**, 21.
- . 1972b, *Ap. J.*, **178**, 1.
- . 1975, *Ap. J.*, **202**, 563.
- Sandage, A., and Hardy, E. 1973, *Ap. J.*, **183**, 743.
- Sandage, A., and Tammann, G. A. 1975, *Ap. J.*, **196**, 313.
- . 1976a, *Ap. J. (Letters)*, **207**, L1.
- . 1976b, *Ap. J.*, **210**, 7.
- Sandage, A., Tammann, G. A., and Hardy, E. 1972, *Ap. J.*, **172**, 253.
- Shapley, H., and Ames, A. 1932, *Harvard Ann.*, **88**, 41.
- Silk, J. 1974, *Ap. J.*, **193**, 525.
- van den Bergh, S. 1960, *Pub. David Dunlap Obs.*, vol. **2**, No. 6.
- Visvanathan, N. 1972, *Pub. A.S.P.*, **84**, 248.
- Visvanathan, N., and Griest, D. 1977, in preparation.

ALLAN SANDAGE: Hale Observatories, 813 Santa Barbara Street, Pasadena, CA 91001

NATARAJAN VISVANATHAN: Mount Stromlo and Siding Spring Observatories, Private Bag, Woden, A.C.T. 2606, Australia